Proceeding Series of the Brazilian Society of Computational and Applied Mathematics, v. 11, n. 1, 2025.

Trabalho apresentado no XLIII CNMAC, Centro de Convenções do Armação Resort - Porto de Galinhas - PE, 2024

**Proceeding Series of the Brazilian Society of Computational and Applied Mathematics**

# Full Euler equations for waves generated by vertical seabed displacements

João Vitor P. Poletto[1]
UFPR, Curitiba, PR

**Abstract**. This work consists on a concise summary of the author's Master's Dissertation. Further details can be found in the original thesis.

We introduce a novel numerical method for simulating surface gravity waves generated by vertical seabed displacements. Our method utilizes a time-dependent conformal map to incorporate seabed geometry and wave profiles, allowing for handling various seabed and wave configurations. We validate our approach by replicating Hammack's tsunami generation and propagation results, confirming accurate wave generation prediction according to Hammack's linear theory. Then, we discuss the effect of nonlinearity on the generated wave. Additionally, we explore limitations of the passive generation approach in the context of the fully nonlinear Euler equations.

**Key words**. Seafloor displacement, Euler equations, Conformal mapping, Pseudo-spectral numerical methods.

## 1 Introduction

In this study, we analyze the generation and propagation of surface gravity waves through underwater seabed displacements. This investigation provides insights into tsunami behavior post-seismic activity [3]. Hammack's seminal research laid the foundation of this topic by devising linear equations to model wave generation, validated through laboratory experiments [9]. His work sparked widespread exploration into surface gravity wave generation using linearized Euler equations as a fundamental model (see [3–5, 10, 19] and references therein).

Recent research on nonlinear waves generated by seabed deformation has primarily focused on asymptotic theory [13, 14] or Reynolds-Averaged Navier-Stokes equations coupled with a $k-\varepsilon$ turbulence model [16, 20]. Michele *et al.* [14] observed that weakly nonlinear models predict waves with higher crests and deeper troughs compared to linear solutions. It is noteworthy that although Lynett and Liu [13] studied fully nonlinear waves, their investigation is made under the assumption of weak dispersion Qi *et al.* [16] and Shen *et al.* [20] noted that nonlinear effects become significant when seabed displacement is high and rapid, underscoring the necessity for comprehensive nonlinear models. The differences between waves generated by linear and nonlinear models warrant further investigation, particularly given the practical implications in engineering and oceanography.

Our aim is to develop a numerical method solving the full nonlinear Euler equations for irrotational flow with two moving boundaries: the seabed and the free surface. The seabed displacement, either upward or downward, initiates surface waves due to geometric deformations of the fluid domain. Our approach involves computing a time-dependent conformal map, transforming the fluid domain into a uniform strip known as the canonical domain. This technique was pioneered by Dyachenko *et al.* [6] and refined by various authors [1, 2, 7, 11, 15, 17].

[1]jvppoletto@gmail.com

 © 2025 SBMAC

The same problem of hydrodynamic that is presented in this work was investigated by Ruban [18]. However, we highlight that our method is more general than the one presented by this author, since our model incorporates seabed variations (in space and time) directly into the physical domain. To the best of our knowledge, this mapping has not been previously reported in the literature within the context of the full Euler equations.

We validate our simulations with Hammack's linearized model. Then we carried out an investigation on the effects of nonlienearites on the generated wave.

This work is organized as follows: The governing equations, the conformal mapping technique and its numerical implementation are presented in Section 2. The numerical experiments are shown in Section 3 followed by our final conclusions and considerations.

# 2 Formulation

We examine an ideal, incompressible fluid with irrotational flow in a channel of finite depth. The time-dependent seabed is represented as $h_0 + h(x,t)$ and the free surface as $\zeta(x,t)$, where $h_0$ denotes a typical depth. Utilizing $h_0$ as the horizontal and vertical length scale and $(gh_0)^{1/2}$ as the velocity scale, we derive the following dimensionless Euler equations.

$$\Delta\phi = 0 \quad \text{for} \quad -1 + h(x,t) < y < \zeta(x,t), \tag{1}$$

$$\phi_y = h_t + \phi_x h_x \quad \text{at} \quad y = -1 + h(x,t), \tag{2}$$

$$\zeta_t + \phi_x \zeta_x - \phi_y = 0 \quad \text{at} \quad y = \zeta(x,t), \tag{3}$$

$$\phi_t + \frac{1}{2}(\phi_x^2 + \phi_y^2) + \zeta = 0 \quad \text{at} \quad y = \zeta(x,t). \tag{4}$$

We supplement these equations with periodic boundary conditions of period $2L$.

Equations (1)-(4) are solved numerically by means of a conformal mapping combined to a pseudo-spectral method which is presented next.

## 2.1 Conformal mapping for a time-dependent seabed

We compute a time-dependent conformal mapping $f(\xi + i\eta, t) = x(\xi,\eta,t) + iy(\xi,\eta,t)$ to flatten the free surface and seabed onto a strip of width $D$. Its components $x(\xi,\eta,t)$ and $y(\xi,\eta,t)$ are harmonic functions of $\xi$ and $\eta$ and the imaginary part of the mapping satisfies the boundary conditions: $y(\xi,0,t) = \mathbf{Y}(\xi,t)$ and $y(\xi,-D,t) = -1 + \mathbf{H}(\xi,t)$ where $\mathbf{H}(\xi,t) = h(x(\xi,-D,t),t)$ contains the information about the bottom corrugations and $\mathbf{Y}(\xi,t)$ contains the information about the instantaneous free surface elevation.

The function $y$ can be written in Fourier series as

$$\begin{aligned} y(\xi,\eta,t) = \mathcal{F}^{-1}_{k_j\neq 0}\left[\frac{-\coth(k_jD)\sinh(k_j\eta)\widehat{\mathbf{H}}}{\cosh(k_jD)}\right] + \frac{1-\widehat{\mathbf{H}}(0,t)}{D}\eta. \\ + \mathcal{F}^{-1}_{k_j\neq 0}\left[\frac{\sinh(k_j(D+\eta))\widehat{\mathbf{Y}}}{\sinh(k_jD)}\right] + \frac{(\eta+D)\widehat{\mathbf{Y}}(0,t)}{D}, \end{aligned} \tag{5}$$

and from the Cauchy-Riemann equations ($x_\xi = y_\eta$) we can write the function $x$ as

$$\begin{aligned} x(\xi,\eta,t) = \mathcal{F}^{-1}_{k_j\neq 0}\left[\frac{i\coth(k_jD)\cosh(k_j\eta)\widehat{\mathbf{H}}}{\cosh(k_jD)}\right] + \frac{1-\widehat{\mathbf{H}}(0,t)}{D}\xi \\ + \mathcal{F}^{-1}_{k_j\neq 0}\left[\frac{-i\cosh(k_j(D+\eta))\widehat{\mathbf{Y}}}{\sinh(k_jD)}\right] + \frac{\widehat{\mathbf{Y}}(0,t)}{D}\xi. \end{aligned} \tag{6}$$

 © 2025 SBMAC

We are denoting the coefficients of the Fourier transform and its inverse respectively by

$$\mathcal{F}_{k_j}[g(\xi)] = \hat{g}(k_j) = \frac{1}{2L}\int_{-L}^{L} g(\xi)e^{-ik_j\xi}\,d\xi \text{ and } \mathcal{F}_{k_j}^{-1}[\hat{g}(k_j)](\xi) = \sum_{j=-\infty}^{\infty} \hat{g}(k_j)e^{ik_j\xi}.$$

The conformal mapping is a periodic function of $\xi$, and we can align its horizontal period with that of the physical problem by selecting a suitable value for $D$. Here, the width of the strip is expressed as $D = 1 - \widehat{\mathbf{H}}(0,t) + \widehat{\mathbf{Y}}(0,t)$.

Let $\mathbf{X}(\xi,t)$ be the horizontal coordinate of the conformal mapping at $\eta = 0$ and $\mathbf{X}_b(\xi,t)$ be its trace along the bottom $\eta = -D$. From (6) we have

$$\mathbf{X}_b(\xi,t) = \xi + \mathcal{F}_{k_j\neq 0}^{-1}\left[i\tanh(k_jD)\widehat{\mathbf{H}}\right] + \mathcal{F}_{k_j\neq 0}^{-1}\left[i\coth(k_jD)\left[\frac{\widehat{\mathbf{H}}}{\cosh^2(k_jD)} - \frac{\widehat{\mathbf{Y}}}{\cosh(k_jD)}\right]\right]. \tag{7}$$

Note that equation (7) defines $\mathbf{X}_b(\xi,t)$ implicitly since $\mathbf{H}(\xi,t) = h(\mathbf{X}_b,t)$. Following Flamarion and Ribeiro [8] we compute $\mathbf{X}_b$ through a fixed point iterative scheme, which considers the topography given directly into the physical domain, unlike Ruban [18].

## 2.2 Euler equations in the canonical coordinates

We use the conformal map as a new coordinate system. Let $\bar{\phi}(\xi,\eta,t) = \phi(x(\xi,\eta,t), y(\xi,\eta,t),t)$ and $\bar{\psi}(\xi,\eta,t) = \psi(x(\xi,\eta,t), y(\xi,\eta,t),t)$ be the velocity potential and its harmonic conjugate in the new variables $\xi$ and $\eta$ and denote by $\mathbf{\Phi}(\xi,t)$ and $\mathbf{\Psi}(\xi,t)$ their values along $\eta = 0$.

Through Euler equations and after some manipulations inspired by the work of Milewski *et al.* [15], we obtain the following uncoupled system

$$\mathbf{Y}_t = \mathbf{Y}_\xi\mathcal{C}\left[\frac{\mathbf{\Psi}_\xi(\xi,t)}{J}\right] - \mathbf{X}_\xi\frac{\mathbf{\Psi}_\xi(\xi,t)}{J}, \tag{8}$$

$$\mathbf{\Phi}_t = \mathbf{\Phi}_\xi\mathcal{C}\left[\frac{\mathbf{\Psi}_\xi(\xi,t)}{J}\right] - \frac{1}{2J}(\mathbf{\Phi}_\xi^2 - \mathbf{\Psi}_\xi^2) - \mathbf{Y}, \tag{9}$$

where $J = \mathbf{X}_\xi^2 + \mathbf{Y}_\xi^2$ is the Jacobian evaluated at $\eta = 0$ and

$$\mathcal{C}\left[\frac{\Psi_\xi(\xi,t)}{J}\right] = \mathcal{C}_0\left[\frac{\Psi_\xi(\xi,t)}{J}\right] - \left\langle \mathbf{X}_\xi\mathcal{C}_0\left[\frac{\Psi_\xi(\xi,t)}{J}\right] + \mathbf{Y}_\xi\frac{\Psi_\xi(\xi,t)}{J}\right\rangle. \tag{10}$$

The notation $\langle\cdot\rangle$ refers to the zero mode of the Fourier Transform.

We calculate the time-dependent conformal map (see equations (5) and (6)) and the evolution of the free surface as depicted above. From given initial conditions $\mathbf{Y}$ and $\mathbf{\Phi}$, these equations are numerically solved using the fourth-order Runge-Kutta method, alongside Fourier spectral discretization for the variable $\xi$, where all derivatives are computed spectrally via the Fast Fourier Transform (FFT). Unless specified otherwise, we employ $N = 2^{12}$ modes in the FFT computation, and the Runge-Kutta method uses a time step of 0.01.

# 3 Numerical experiments

We are interested in studying flows in which the seabed movement is characterized by a section of the seabottom moving vertically either up or down. For this purpose, we consider a fluid

DOI: 10.5540/03.2025.011.01.0518  © 2025 SBMAC

domain of approximately 200 times the depth of the channel. In the middle of the domain the seabed displacement is given by the function

$$h(x,t)=\begin{cases}\dfrac{z_0\,(1-\cos(\pi t/T))\,\big(1+\tanh(\mu(b^2-x^2))\big)}{2\,(1+\tanh(\mu b^2))} & t\leq T,\\[2ex] \dfrac{z_0\,\big(1+\tanh(\mu(b^2-x^2))\big)}{1+\tanh(\mu b^2)} & t>T.\end{cases} \tag{11}$$

Note that when $t = T$ the elevation (or depression) of the seabed stops and it reaches its maximum displacement $z_0$. Unless mentioned otherwise, we use $\mu = 0.4$. Furthermore, we approximate the boundary conditions by periodic ones.

## 3.1 Benchmark

As shown in the seminal work of Hammack [9], the solution of the linearized version of the equations (1)-(4) is $\zeta(x,t)=\mathcal{F}^{-1}\left[\mathrm{sech}(k_j)\int_0^t \cos(\omega_j(t-s))\hat{h}_t(k_j,t)ds\right]$, where $\omega_j^2 = k_j \tanh(k_j)$.

The sea bed elevation (11) is controlled by three parameters: $z_0$, $b$ and $T$. In this work, we shall present the case related to the impulsive displacement, where $b = 6.1$ and $T = 0.793$. We compare the free surface waves computed from the system (8)-(9) with those taken from Hammack's model. The models are quite similar especially during the wave generation phase for small topography amplitudes. See figure 1, which shows the relative error between the nonlinear solution ($\zeta_E$) to the linear one ($\zeta_L$) in respect to time, computed by the formula $E(t) = \|\zeta_E(\cdot,t)-\zeta_L(\cdot,t)\|_2/\|\zeta_L(\cdot,t)\|_2$.

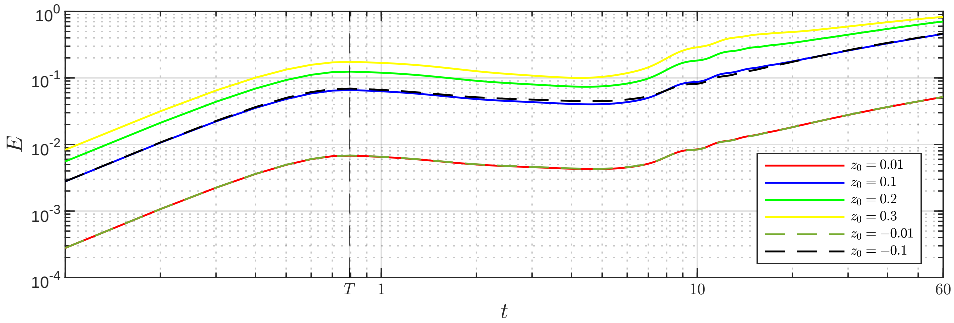


Figure 1: Relative difference between nonlinear and linear solutions versus time for the impulsive regime, considering different values of $z_0$.

## 3.2 Similarities and differences: linear vs. nonlinear model

Figure 2 displays four snapshots of the wave dynamic. During the generation phase, both models exhibit similar behavior. However, nonlinear effects become apparent later on, with the nonlinear wave propagating faster than the linear one. By $t = 60$, the nonlinear solution appears less smooth compared to Hammack's model.

When the seabed submerges the inverse phenomenon happens, the nonlinear solution is slower than the linear one which is just a reflection along the $x$ axis of the solution obtained from the platform ascending. In order to show the different speeds of propagation we plot the linear and non linear solutions at $t = 28$ for $|z_0| = 0.3$ (see figure 3). The solution corresponding to the sinking seabed has been reflected around the $x$ axis for comparison.

 © 2025 SBMAC

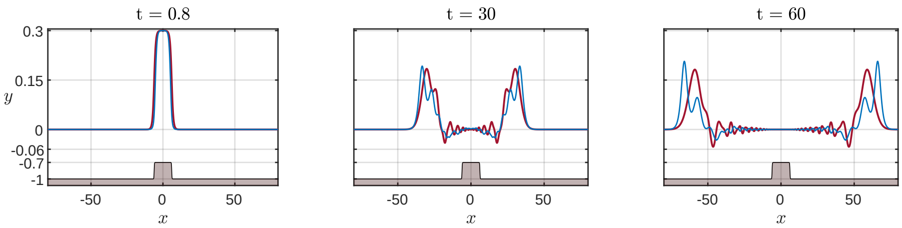


Figure 2: Snapshots of the waves generated for both models. Blue line: solution of the Euler equations. Red line: solution of the linear model of Hammack. Black line: seabed. Parameter: $z_0 = 0.3$.

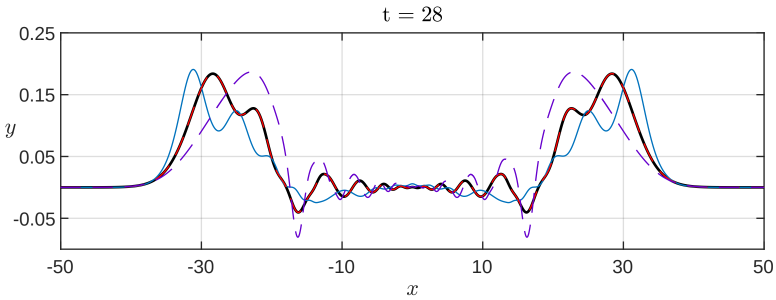


Figure 3: Symmetry comparison with respect to $x$-axis. Blue-solid line refers to the nonlinear solution obtained via the platform lifting and purple-dashed line represents the opposite of the nonlinear solution via the platform lowering. The linear solutions are represented by the red and black colors. Parameter: $z_0 = 0.3$.

### 3.3 Passive and active generation

A traditional method for studying waves generated by a moving seabed involves translating the seabed deformation to the free surface and propagating it, after the seafloor stabilizes into its final position. This technique is known as *passive generation*. Conversely, when seabed motion is directly integrated into wave generation, it is called *active generation* [4]. We explore the disparities between passive and active generation within the framework of the full Euler equations. Previous research in this area has primarily focused on the linear wave regime [4, 12], indicating that passive generation is viable under conditions of rapid seabed displacement.

We present snapshots of wave dynamics in Figure 4. These snapshots reveal that while the passive approach accurately captures the leading wave dynamics, it fails to predict subsequent wave behavior, resulting in a spurious oscillatory tail. The error from passive generation was approximately 16% relative to the solution obtained through active generation.

## 4 Conclusion

In this work, we presented a novel numerical method for solving the full Euler equations in the presence of variable spatial and temporal topography, utilizing the conformal mapping technique and spectral numerical methods. To validate our approach, we compared its predictions with solutions obtained from Hammack's linear model. Both models exhibited good qualitative agreement for small topography displacements. However, for larger seabed displacements, significant differ-

DOI: 10.5540/03.2025.011.01.0518  © 2025 SBMAC

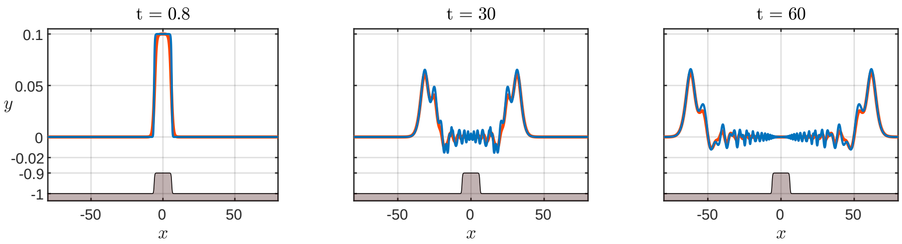


Figure 4: Snapshots of the nonlinear waves generated for passive and active approach. Blue line: passive generation. Orange line: active generation. Black line: seabed. Parameters: $z_0 = 0.1$ and $\mu = 0.2$.

ences emerged, especially during the propagation phase. Additionally, we demonstrated that the nonlinear solution displays a non-symmetric profile with respect to the $x$-axis, contrasting with the linear case.

Moreover, our investigation delved into passive generation, revealing that while this method accurately captures the dynamics of the leading wave, it falls short in predicting subsequent wave behavior.

Our method's capability to handle nonlinear dynamics extends its applicability to a broad spectrum of problems, including landslides, interactions of solitary waves with variable-speed obstacles, and other scenarios featuring complex topographies. Furthermore, the combination of conformal mapping and spectral methods offers opportunities to explore diverse fluid dynamics and wave propagation challenges in demanding environments such as coastal regions, underwater structures, and atmospheric conditions. This not only deepens our comprehension of natural phenomena but also facilitates practical applications in engineering and environmental studies. The ability to address nonlinear dynamics and complex topographies enhances the significance and utility of the numerical methods outlined in this study across various scientific disciplines, contributing to a comprehensive understanding of natural processes and supporting practical applications in engineering and environmental research.

## Acknowledgments

This work was supported by the the Coordenação de Aperfeiçoamento de Pessoal de Nível Superior - CAPES. The author thanks his advisor, Professor Roberto Ribeiro-Jr, and his co-advisor, Professor Francisco de Melo Viríssimo. Additionally, the author acknowledges the contributions of Professors David Andrade and Marcelo V. Flamarion to the development of this work.

## References


[1] D. Andrade and A. Nachbin. “Two-dimensional surface wave propagation over arbitrary ridge-like topographies”. In: **SIAM Journal on Applied Mathematics** 78.5 (2018), pp. 2465–2490.

[2] W. Choi and R. Camassa. “Exact evolution equations for surface waves”. In: **Journal of engineering mechanics** 125.7 (1999), pp. 756–760.

[3] D. Duthyk and F. Dias. “Tsunami generation by dynamic displacement of sea bed due to dip-slip faulting”. In: **Mathematics and Computers in Simulation** 80.4 (2009), pp. 837–848.


 © 2025 SBMAC

[4] D. Dutykh, F. Dias, and Y. Kervella. “Linear theory of wave generation by a moving bottom”. In: **Comptes Rendus Mathematique** 343.7 (2006), pp. 499–504.

[5] D. Dutykh, D. Mitsotakis, X. Gardeil, and F. Dias. “On the use of the finite fault solution for tsunami generation problems”. In: **Theoretical and Computational Fluid Dynamics** 27 (2013), pp. 177–199.

[6] A. I. Dyachenko, V. E. Zakharov, and E. A. Kuznetsov. “Nonlinear dynamics of the free surface of an ideal fluid”. In: **Plasma Physics Reports** 22.10 (1996), pp. 829–840.

[7] M. V. Flamarion, T. Gao, R. Ribeiro-Jr, and A. Doak. “Flow structure beneath periodic waves with constant vorticity under normal electric fields”. In: **Physics of Fluids** 34.12 (2022).

[8] M. V. Flamarion and R. Ribeiro-Jr. “An iterative method to compute conformal mappings and their inverses in the context of water waves over topographies”. In: **International Journal for Numerical Methods in Fluids** 93.11 (2021), pp. 3304–3311.

[9] J. L. Hammack. “A note on tsunamis: their generation and propagation in an ocean of uniform depth”. In: **Journal of Fluid Mechanics** 60.4 (1973), pp. 769–799.

[10] T. Jung and S. Son. “Active tsunami generation by tectonic seafloor deformations of arbitrary geometry considering rupture kinematics”. In: **Wave Motion** 100 (2021), p. 102683.

[11] Y. A. Li, J. M Hyman, and W. Choi. “A numerical study of the exact evolution equations for surface waves in water of finite depth”. In: **Studies in applied mathematics** 113.3 (2004), pp. 303–324.

[12] C. M. Liu. “Analytical solutions of tsunamis generated by underwater earthquakes”. In: **Wave Motion** 93 (2020), p. 102489.

[13] P. Lynett and P. L.-F. Liu. “A numerical study of submarine–landslide–generated waves and run–up”. In: **Proceedings of the Royal Society of London. Series A: Mathematical, Physical and Engineering Sciences** 458.2028 (2002), pp. 2885–2910.

[14] S. Michele, E. Renzi, A. G. L. Borthwick, C. Whittaker, and A.C. Raby. “Weakly nonlinear theory for dispersive waves generated by moving seabed deformation”. In: **Journal of Fluid Mechanics** 937 (2022), A8.

[15] P. A. Milewski, J. M. Vanden-Broeck, and Z. Wang. “Dynamics of steep two-dimensional gravity–capillary solitary waves”. In: **Journal of Fluid Mechanics** 664 (2010), pp. 466–477.

[16] M. Qi, Y. Kuai, and J. Li. “Numerical simulation of water waves generated by seabed movement”. In: **Applied Ocean Research** 65 (2017), pp. 302–314.

[17] R. Ribeiro-Jr, P. A. Milewski, and A. Nachbin. “Flow structure beneath rotational water waves with stagnation points”. In: **Journal of Fluid Mechanics** 812 (2017), pp. 792–814.

[18] V. P. Ruban. “Water waves over a time-dependent bottom: Exact description for 2D potential flows”. In: **Physics Letters A** 340.1-4 (2005), pp. 194–200.

[19] T. Saito. “Dynamic tsunami generation due to sea-bottom deformation: Analytical representation based on linear potential theory”. In: **Earth, Planets and Space** 65 (2013), pp. 1411–1423.

[20] Y. Shen, C. N. Whittaker, E. M. Lane, W. Power, and B. W. Melville. “Interference effect on tsunami generation by segmented seafloor deformations”. In: **Ocean Engineering** 245 (2022), p. 110244.

DOI: 10.5540/03.2025.011.01.0518

© 2025 SBMAC